



*Journal of Advances in
Science and Technology*

*Vol. III, Issue No. VI,
August-2012, ISSN 2230-
9659*

**INTERACTION FOR EXTERNAL AERODYNAMICS
AIRFOIL COMPUTATIONS WITH VISCOUS
INTERACTION**

AN
INTERNATIONALLY
INDEXED PEER
REVIEWED &
REFEREED JOURNAL

Interaction for External Aerodynamics Airfoil Computations with Viscous Interaction

Rakesh Kumar^{1*} Dr. R. K. P. Yadav²

¹ Research Scholar

² Professor & Head, Department of Physics, B. N. Mandal University, Madhepura

Abstract – Mat FOIL has been developed to model low-speed airfoils quickly and reliably under various airfoils of flow conditions. The method is based on the second order of the viscous vortex possible flow method and the displacement thickness iterative method is right for the viscous effect. The viscous correction is based on an integral formula of two equations, assisted by many empirical correlations and closing relationships. The possibility of simulating the effects of ground proximity is perhaps the most beneficial software module. A mirror image vortices distribution models the influence of the ground effect. The software is used to reliably predict parametric reliance on arbitrary aerodynamic coefficients near the ground. Favorable and unfavorable soil effects that are not at least contingent on the operating height of the airframe above the surface are expected. Interaction for external airfoil aerodynamics with viscous interaction is discussed in this paper.

Key Words – Interaction, Aerodynamics, Airfoil, Viscous Interaction, Software Package, Arbitrary, Vortex Potential Flow.

-----X-----

INTRODUCTION

Wing in Ground (WIG) craftsmen claim to fly more technically because of the impact of the close proximity to ground or water surfaces. Wing in Ground This could result in an extremely cost-efficient way of transport by flying In Ground Effect (IGE). Due to the demand for relatively high-speed sea transport, Ultra Heavy Lift Aircraft (UHLA) and efficient military / special operations, researchers and aerodynamics are intensively researching the lifting, dragging and longitudinal stability effects of land and free water surfaces on the WIG work. In addition to the favourable aerodynamic benefits, WIG crafts give endless military and civil operational benefits over hydrofoils and surface handlers. WIG craft has very low acoustic signature as well as a limited detection range compared to traditional aircraft while operating at extremely low altitude. The relative speed advantage over normal sea ships guarantees rapid dispersion and survival. The improvement in aerodynamic efficiency is due both to an increase in height and a decrease of the drag, normally up to an altitude of the entire wing length of the plane. Land proximity greatly increases airfoil lifting because of the impact known as the chord wise. The interaction with a flat surface compresses the airfoil's lower surface streamlines to create high static pressure. In addition, the development of wing spike vortices is disrupted, which compresses the vortices and greatly reduces their forces, decreasing the lifting drag. The span-wise

effect is generally called this. For several decades there have been theoretical and experimental analyses of the terrestrial effects that are based on the approximation theory developed by Wiesel's berger[6] in 1922. In addition , the two events were believed to be distinct and could be viewed individually. In fact, nonlinear interactions between chord wise and span wise effects do not allow the combined effect to be calculated by simply superposing the wise and span wise results of the chord, as is underlined in the accompanying report[5]. The chord dominant impact will lead to a variety of positive and adverse effects through contact with the surface of the earth, the airfoil geometry and the formation of the boundary layer. For example, many airfoils display a Venture effect (see Figure 1) that produces a high speed area. The pressure reduction causes the suction of the field, which in many cases is sufficiently high to minimise the lifting coefficient. This phenomenon normally happens in the regime of intense soil impact (h / c bis0.2). In order to correctly form the lower surface profile geometry, the adverse effects of suction can be counteracted to limit the flux variance of the floor-bound volume. With regard to airfoil longitudinal stability, it may be prudent to suck the airfoil so that it does not heavily load its leading or trailing edges. With the development of reflexed and s-shaped section airfoils, designers can work in conditions of intense soil-effect without a great varying pitching period.

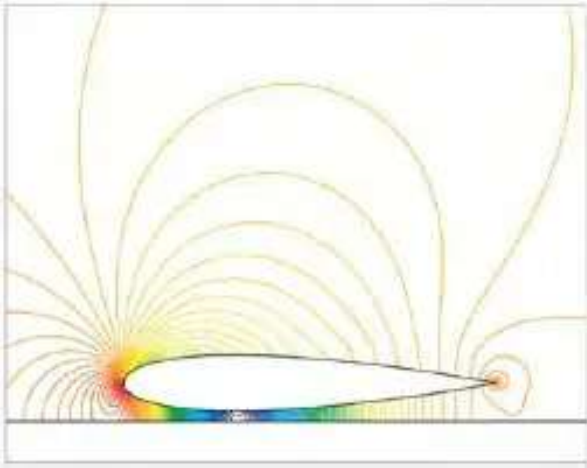


Figure 1. NACA 0015 airfoil in extreme ground effect ($h/c = 0.1$) exhibiting the 'Venturi Effect' due to ground-induced suction

Recent advances in numerical and computer analytics technology allowed the study of the terrestrial effect using the Navier-Stokes Equations as the physical phenomenon mathematical model. However, this is still a laborious method, and a simpler approach remains important to achieve fast and relatively accurate solutions. The solution can be greatly simplified by using a constant potential flow and integrated boundary layer theory for numerical simulation of the performance and flow fields of the airfoil sections in the ground effect. Since fluid movements around an airfoil IGE are more lengthy than in unbound flux fields and since the formation of boundary layers affects the pressure distribution considerably, there is an interaction scheme. In viscous and viscous solutions are related to the methods of literature iteratively by the displacement thickness [2,3]. In order to allow the user to evaluate multiple airfoil for a preliminary design calculation comparison purposes, a graphical user interface (GUI) has also been developed.

VISCOUS-INVISCID FORMULATION

Literature has been very detailed in describing the foundations of possible flow theory [3,4]. The selection of a single element in order to solve the Laplace equation involves potential flow theory. It is enough to say here that the disruption of the free flow due to a fluid is modelled by putting vortex boards that reflect the form of the airfoil within the free flow. A continuous, linear curve is the form of the airfoil, connecting the points on the surface of the airfoil. The distributed vorticity or vortex intensity per unit length is shown in each column. Since the panel is partially linear, the vorticity is believed to be distributed linearly along each panel. The speed at the control point (located at the midpoint of the panel) is measured by measuring the effect of the singularity of the vortex around the airfoil.

The chosen limits are then added to indicate the flow direction so that the fluid does not enter the surface.

The strengths of each vortex are then determined by taking into account the contribution of each variable induced speed. During the process of iteration, a possible flow solver is used until the effect of the μl * displacement thickness is applied to determine the pressure distribution over the airfoil. The existence of the border layer reveals now a finite thickness of the trailing border. The pressure reduction on the trailing edge increases the drag due to the presence of the limit sheet. A wakeboard with constant vortex strength is considered to effectively model the impact of a blunt trailing edge.

To simulate the soil effect, a mirror image vortex panel distribution is used. A secondary velocity portion of any panel of the actual airfoil is generated by the imaginary vortex distribution below the soil. The free current is held along the x axis and the airfoil is rotated in the clockwise direction at an angle β around the trailing edge. The rotated airfoil form is then moved up by a quantity of (h / c) , where h is the height of the edge above the field.

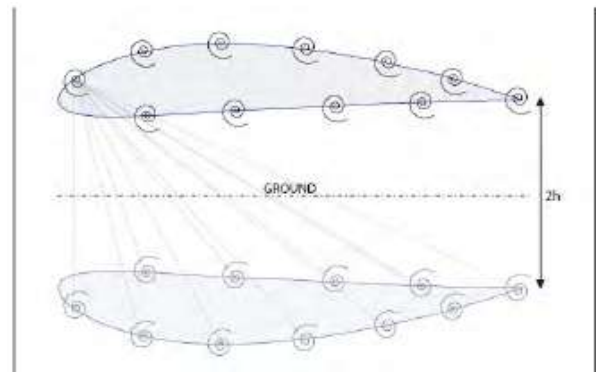


Figure 2. Chord wise ground effect representation through image vortex distribution

BOUNDARY LAYER MODULE

This process is used to accurately calculate the velocity distribution over the airfoil surface using the panel method mentioned previously. The velocity distribution is then used to determine that the boundary layer is grown on the airfoil surface and then applied to the original inviscid pressure distribution by applying viscous boundary layer corrections. The Prandtl method is an integral layer method to the boundary. The fluid flow equations are based on mass, dynamism and energy conservation principles. The flow field is expected to be incompressible all along and the surface-free flux temperature variations are insignificant and thus the fluid density ρ , and the dynamic viscosity μ , can be considered constant in the conservation equations.

AIRFOIL- SHOCK-WAVE INTERACTION: GENERATION OF A VORTEX

The airfoil-shock-wave interaction phenomenon will start when the shock is on the lead airfoil. After the shock wave has affected the airfoil, a wave of

reflections that propagate all directions is produced. As it is noted in Figure 5, the reflecting wave appears to be stronger than the lower one in the upper tube area because the effect on the upper surface of the aerial foil has been high. The time sequence of the resulting stream field as shown in Figure 6 indicates that the shock wave is then divided into two parts. The upper shock wave near the airfoil surface is seen to be more fast than the lower one because of the inclination of the airfoil and the reflected pressure wave. The high shock first arrives at the trailing edge of the airfoil, as predicted. The lower is around 0.03ms delayed. The upper shock is heading backwards below the trailing edge of the airfoil during this short duration and is almost responsible for forming the starter vortex. When the lower shock enters the trail, the combined shock system continues in the direction of the rear airfoil with the new vortex near at its heels. The history of the shock crossing following the formation and subsequent separation of the vortex at trailing edge is graphically shown in Figure 3 (c – e).

As a result of the interaction between the airfoil and shock-wave, the lead airfoil produces two distinct waves of compression. The vortex has drifted down the lead airfoil at free flow speed after 0.51 ms (after impact), as shown in Figure 3(f). After 1.05 ms into flow history, the flow began to be separated from the underlying airfoil and turbulence, especially at the inner centre of the vortex, was apparent from the turbulent viscosity contours of Figure 7. Figure 4 shows the contour of the flow field at the moment when the shock wave passes approximately halfway past the back of the airfoil. The lead airfoil is produced with the shock hitting the airfoils by a similar reflection compressibility wave. The vortical flow activity is the most fascinating thing. The vortex is almost symmetrical, as seen in the experiment[3]. Also above the vortex is observed a downward reflection compressibility wave. This wave represents the wall of the original compression wave generated during the interaction between lead-airfoil and vortex.

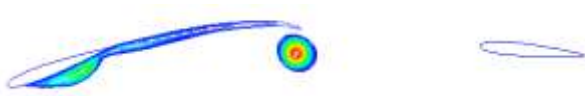


Figure 3: Turbulent viscosity at t = 1.05ms

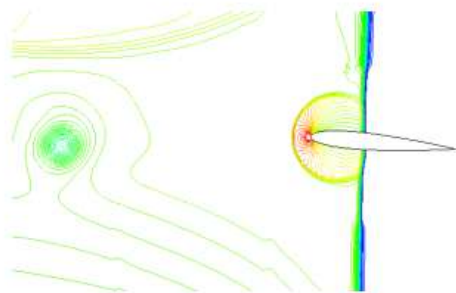


Figure 4: Pressure distribution at t = 1.05 ms when the shock wave passes over the aft airfoil

Figure 5 gives a description of the flow activity in the shock tunnel. A massive flow separation at the lower side of the lead airfoil is observed at this moment, $t = 1,35$ ms. The oblique wave of incident compression reflected from the top wall can now be clearly seen. The presence of the vortex and the rear airfoil disturbs the pressure wave. This helps to improve flow insecurity. There are also two other waves of circular compressibility from the rear airfoil. The first was due to the impaction of the shockwave on the airfoil's head end and the second was generated when the shockwave left the trailing edge. Figure 6 demonstrates the turbulent viscosity and vorticity contours of the flowfield. The vortex was found to be accompanied by the lead airfoil wake when leaving the trailing edge of the lead airfoil. This wake extends to a series of small vortices along the wake track (not seen here). This does not have a serious effect on the AVI process because it is in the shadow of the more strongly formed vortex.

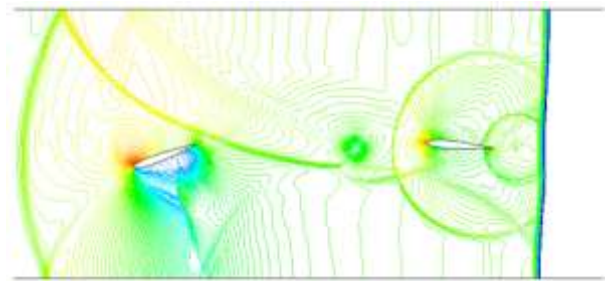


Figure 5: Global view of the pressure distribution within the shock tube at t = 1.35 ms

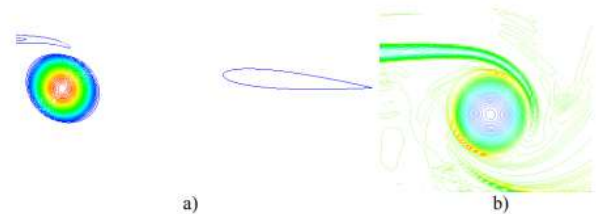


Figure 6: Contours of turbulent viscosity a) and vorticity b) at t = 1.35 ms

AIRFOIL-VORTEX INTERACTION (AVI)

Figure 7 gives a close view of the contours of pressure around the airfoil at various times. The AVI process starts when the vortex is situated near the aft edge of the airfoil. Figure 7(a) indicates that as the vortex crosses through it, the wave of compressibility is severely affected. Circulation of the vortex is on the horizontal direction; hence downwash affects the flow above or at the airfoil 's edge. In consequence the point of stagnation is moved to the top of the airfoil, which is at a 5 degree angle of attack. When the flow under the airfoil accelerates, beneath the leading edge there is a supersonic flow accompanied by a shock wave. The downwash flow is strengthened as the vortex travels forward, as seen in Fig . 7(b), and the stagnation point is inverted along the top of the

airfoil. The compression wave is seen travelling along the airfoil surface as a consequence of the movement of the running shock wave on the trailing edges. The distance between the vortex centre and a horizontal line through the airfoil is approximately $-0.14c$. The flow patterns of the vortex are shown to be greatly affected as it travels near the lower surface of the airfoil (see Figures 7c and d, among other things). In this case, due to the flow acceleration induced by the vortex, the low pressure area extends underneath the airfoil. This creates a downward boost. The vortex interaction on the airfoil is followed by the creation of a compressibility wave on the edge of the airfoil. In Figures 7 (e-f), this wave, considered to be a source of noise, can be seen clearly.

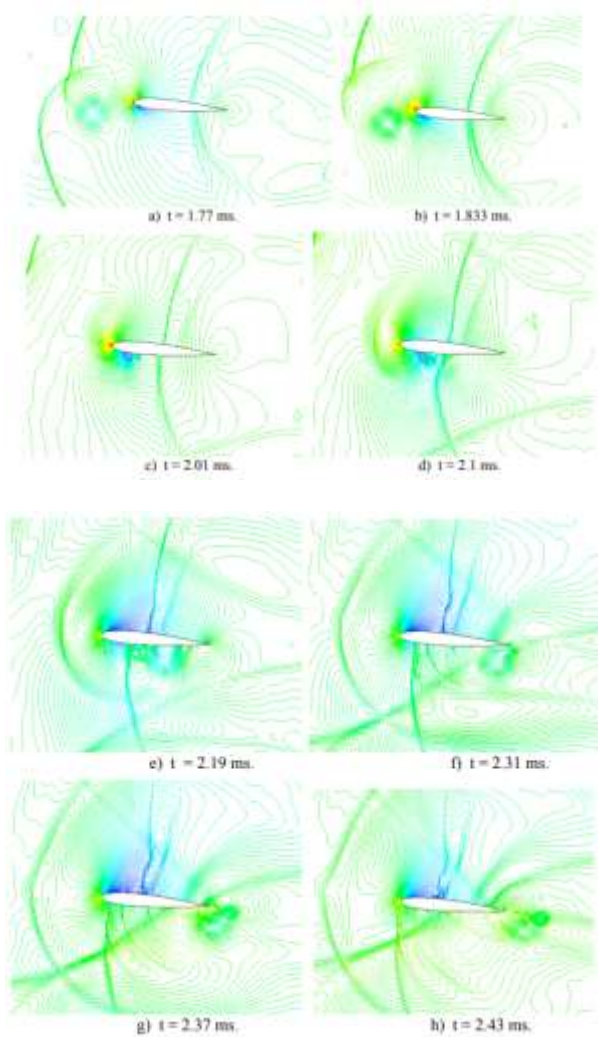


Figure 7: Airfoil-Vortex Interaction process: Pressure distribution contours

As the vortex comes close to the halfway underneath the airfoil its impact on the upper surface is diminished by the physical shielding of the airfoil and by its finite angle of attack, its flow begins to pace. This eventually restores the elevator. In addition, the dominant shock wave at the top appears to remain stationary, while the shock is seen to pass upstream at the bottom surface (see Figure 7 e-h). The vortex intensity is reduced in the AVI process, but the resulting sharpness in the wake creates a secondary vortex on the rear edge of

the airfoil. The vortices are considerably dissipated, particularly by the rough grid effects, two chords downstream. Figure 8 displays the time history of the C_L aft airfoil elevator. In the same Figure, for comparison, results of experiments obtained for the mis-distance of $h / c = -0.1$ are presented. The experimental results are in line with the moving shockwave that comes to a $t = 1$ ms at the front. The lift increases gradually as the shock wave travels past the airfoil, since the airfoil is at a given angle of attack. The first peak (maximum) on the curve marks the arrival, which contributes to a decrease in elevation, of the reflected compressibility wave. If the wave of compressibility moves through the aft airfoil, the rise begins at about $t = 1,6$ ms. The vortex is at this moment near the airfoil 's leading edge, reaching another height (second peak). The lift is seen to decrease to $t = 2$ ms as the vortex begins to interact with the airfoil structure. At this moment the lift is decreased to a negative value of around $C_L = -0.5$ (downward force). The raise seems to rebound rapidly as the vortex leaves the airfoil. The compressible reflection wave from the lower wall raises the lift faster than the effects of the experiment. The time history of the lift as shown in Figure 8 can be shown to qualitatively be well-aligned with the experimental results during the AVI method, modelled on the current simulations, where the miss-distance was measured at around $0.14[3]$. The slight disparity between the current simulations and the experiment results possibly stems from reflective waves that are suppressed by triangle slates on top and bottom walls of the tube during the experiment.

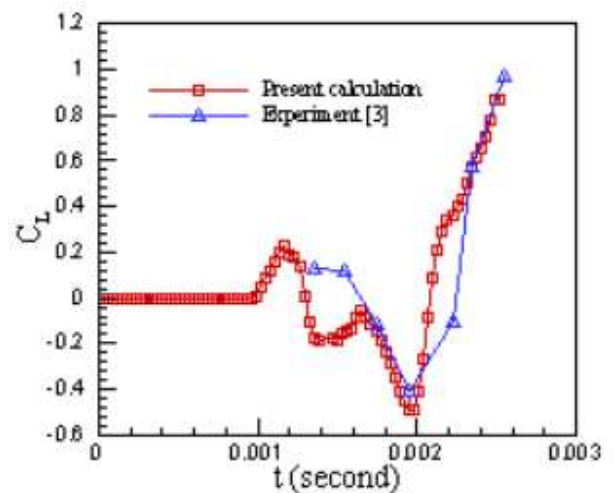


Figure 8: Time history of the lift coefficient C_L for the aft airfoil. Qualitative comparison with experimental data

CONCLUSION

This study addressed the development of an airfoil analysis viscous-inviscid algorithm for ground impact modeling. The solver incorporates updated methods of the potential flow vortex with two detailed formulations for the viscous correction. The transformation is estimated with the method of the disruption

amplification ratio. A fair correlation for the unlimited free stream solution was seen with experimental knowledge, although there was some discrepancy. This is seen as a drawback of the approximation of the panel system. The correlation is really strong with the Euler wording. The programme has shown the beneficial and harmful effects of ground proximity to allow parametric optimization or preliminaries to be performed for ground effect studies.

REFERENCES

1. Caradonna, F. X. (1990). "The Application of CFD to Rotary Wing Flow Problems", AGARD-R781.
2. Piechna, J. and Szumowski, A. P. (1998). "Effect of Miss-Distance on the Airfoil-Vortex Interaction: Numerical study", Arch. Mech., 50, 1, Warazawa, pp. 127-138.
3. Sobieraj, G., Piechna, J., Selerowicz, W. and Szumowski, A. P. (1998). "Effect of Angle of Attack on the Airfoil-Vortex Interaction", The Arch. Mech. Eng., XLV, 1, pp. 19-30.
4. Petrini, E., Efraimsson, G. and Nordstrom, J. (1998). "A Numerical Study of the Introduction and Propagation of a 2-D Vortex", The Aeronautical Research Institute of Sweden, FFA TN 1998-66.
5. Kaminski, W. S. and Szumowski, A. P. (1995). "Acoustic Effects of Parallel Vortex-Airfoil Interaction", Journal of Sound and Vibration, Vol. 183, No 2, pp. 209-220.
6. Selerowicz, W., Sorbieraj, G. and Szumowski, A. P. (1998). "Effect of Miss-Distance on the AirfoilVortex Interaction: Experiment", Arch. Mech., 50, 1, Warazawa, pp. 691-701.
7. Wittmer, K. S. and Devenport, W. J. (1999). "Effects of Perpendicular Blade-Vortex Interaction, Part. 1: Turbulence Structure and Development", AIAA Journal, Vol. 37, No. 7, pp. 805-812.
8. Wittmer, K. S. and Devenport, W. J. (1999). "Effects of Perpendicular Blade-Vortex Interaction, Part. 2: Parameter Study", AIAA Journal, Vol. 37, No. 7, pp. 813-817.
9. Spall, R. E. (2001). "Numerical Study of a Wing-Tip Vortex Using the Euler Equations", Journal of Aircraft, Vol. 38, No. 1, pp. 22-27.
10. Ravi, S., Winarto, H., Carrese, R., Louli, Z. (2008). Combined Chordwise and Spanwise Effects Acting on a Wing Near the Ground, IJSE.

Corresponding Author

Rakesh Kumar*

Research Scholar

anu906056@gmail.com